

In-situ measurements of the mixing state and optical properties of soot with implications for radiative forcing estimates

Ryan C. Moffet^a and Kimberly A. Prather^{b,1}

^aLawrence Berkeley National Laboratory, 1 Cyclotron Road, Berkeley, CA 94720; and ^bDepartment of Chemistry and Biochemistry, University of California, San Diego, and Scripps Institute of Oceanography, La Jolla, CA 92093

Edited by Mark H. Thiemens, University of California, San Diego, La Jolla, CA, and approved May 29, 2009 (received for review January 10, 2009)

Our ability to predict how global temperatures will change in the future is currently limited by the large uncertainties associated with aerosols. Soot aerosols represent a major research focus as they influence climate by absorbing incoming solar radiation resulting in a highly uncertain warming effect. The uncertainty stems from the fact that the actual amount soot warms our atmosphere strongly depends on the manner and degree in which it is mixed with other species, a property referred to as mixing state. In global models and inferences from atmospheric heating measurements, soot radiative forcing estimates currently differ by a factor of 6, ranging between 0.2–1.2 W/m², making soot second only to CO₂ in terms of global warming potential. This article reports coupled in situ measurements of the size-resolved mixing state, optical properties, and aging timescales for soot particles. Fresh fractal soot particles dominate the measured absorption during peak traffic periods (6–9 AM local time). Immediately after sunrise, soot particles begin to age by developing a coating of secondary species including sulfate, ammonium, organics, nitrate, and water. Based on these direct measurements, the core-shell arrangement results in a maximum absorption enhancement of 1.6× over fresh soot. These atmospheric observations help explain the larger values for soot forcing measured by others and will be used to obtain closure in optical property measurements to reduce one of the largest remaining uncertainties in climate change.

aerosol | atmosphere | climate | composition

Soot particles represent the most strongly absorbing class of atmospheric aerosol at visible wavelengths and thus may warm the earth's surface directly by absorbing the incoming radiation from the sun. The direct forcing by soot depends not only on its optical properties but also on the altitude of the layer and the amount of reflection from below. Furthermore, when soot is deposited, it can accelerate the melting of ice and snow. Indirectly, soot can alter climate by heating the atmosphere and changing atmospheric dynamics, or by serving as nuclei for cloud formation, thereby changing cloud properties (1, 2). Not surprisingly, the importance of soot to climate change has been a major focus of many modeling, laboratory, and field studies (3–10). Recent investigations involving direct atmospheric measurements of soot particles suggest that they may have a global warming potential second only to CO₂ (11–13). The aforementioned modeling studies predicting higher radiative forcing values model soot particles as a core of strongly absorbing soot surrounded by a nonabsorbing shell. However, large uncertainties still exist in estimates of the radiative forcing of soot because of the lack of detailed in situ measurements of the mixing state and the associated optical properties as a function of particle size. These uncertainties limit our ability to quantify the relative impacts of soot on climate, thus limiting our ability to make effective policy decisions (14).

To reduce the uncertainties associated with atmospheric soot particles, direct measurements are required to quantify the chemical, physical, and optical characteristics of soot. The

optical properties of soot are very sensitive to the manner in which each particle is mixed with other species such as condensed organic carbon, sulfate, nitrate, and water. As soot particles age, they become coated by nonabsorbing species produced as a result of gas-phase oxidation reactions. Many studies suggest the use of a single particle optical model of an absorbing spherical core surrounded by a mantle of nonabsorbing material is appropriate for aged aerosol (5, 8, 14). Based on modeling and laboratory studies, a strongly absorbing soot particle surrounded by a nonabsorbing shell has been shown to enhance particle absorption by up to a factor of 3 (4, 15–18). In these cases, the use of the core-shell model serves as an excellent model system for aged aerosols. However, for fresh soot aerosols, such core-shell models may be unreliable for accurately predicting the optical properties of highly nonspherical particles with small coatings (5, 16, 19). Thus, it is crucial to determine how long it takes freshly emitted soot particles in an urban environment to convert to aged coated spheres to confidently predict atmospheric heating rates by using the core-shell assumption.

Measurements have been advancing so that it is possible to determine the detailed structure and chemical composition of soot particles. Using coupled incandescence and scattering at infrared wavelengths, coated soot particles can be inferred in real-time (20). Detailed measurements of the chemical composition and morphology of soot can be obtained with electron microscopy techniques (21, 22). These measurements support the use of modeling soot as an internal mixture with core-shell morphologies. However, microscopy techniques are performed in the laboratory and in a vacuum, which can change the morphology of the soot particles due to how they are impacted on the substrate; evaporation of water and other semivolatile species may also occur. Furthermore, the counting statistics provided by particle microscopy are often limited and thus may not be fully representative of ambient soot particles.

Over the past decade, mass spectrometers have been developed to measure the chemical composition and size of single atmospheric soot particles in real-time by using a combination of aerodynamic sizing and laser desorption ionization mass spectrometry. A most recent and promising advance in single particle mass spectrometry yields aerosol optical properties by measuring the intensity of scattered light as each particle passes through lasers originally used for aerodynamic sizing. These optical measurements have been applied to nonabsorbing ambient particles with different chemical mixing states and modeled by using Mie theory, thereby providing refractive index and density information (23). In this report, these in situ measurements of

Author contributions: R.C.M. and K.A.P. designed research, performed research, analyzed data, and wrote the paper.

The authors declare no conflict of interest.

This article is a PNAS Direct Submission.

¹To whom correspondence should be addressed. E-mail: kprather@ucsd.edu.

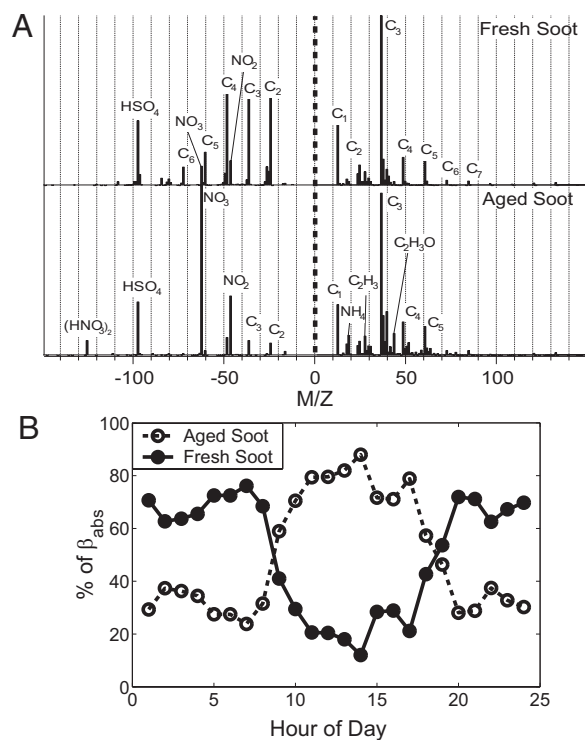


Fig. 1. Single particle mass spectra and a time series showing the contribution to absorption coefficient (β_{abs}) by fresh and aged soot in Mexico City. (A) Average fresh and aged soot particle mass spectra from Mexico City derived from the clustering analysis. For fresh soot (*Upper*), elemental carbon ion clusters (C_n^\pm) represent the most intense peaks. For aged soot (*Lower*), the most intense peaks are due to condensed species resulting from photochemistry [nitrate ($m/z - 62$), sulfate ($m/z - 95$), and organic species ($m/z 27, 43$)]. (B) Average diurnal contribution of fresh and aged soot particles to the absorption coefficient in Mexico City. Fresh soot particles account for the majority of the absorption coefficient in the early morning and at night because of emission patterns and the absence of photochemistry. Aged soot particles are responsible for the majority of the midday absorption when the solar irradiance is higher.

the size-resolved mixing state and optical properties are described for atmospheric soot particles in two different urban locations, Riverside, CA, and Mexico City, Mexico. Detailed measurements of the optical, size-resolved chemical mixing state and microphysical properties for ambient soot particles are compared with the core-shell optical model. Moreover, the timescale is directly measured for transformation of atmospheric soot particles from fresh fractal morphologies to aged spherical particles in photochemically active urban atmospheres.

Identification of Fresh and Aged Soot. In Riverside and Mexico City, single particles were classified based on chemical composition. Two distinct types of soot particles were identified based on differences in their mass spectral ion intensity patterns (Fig. 1A). Previous lab studies have shown how these mass spectral ion signatures can be used to assess the age of soot particles; it was found that carbon cluster ions ($C_n^{+/-}$) dominate the mass spectra for fresh soot particles as shown in Fig. 1A *Upper*. For aged soot particles, shown in Fig. 1A *Lower*, photochemically produced secondary species such as organic carbon (OC) and nitrate are found in the same particle (internally mixed) as the soot.

It is important to point out that the majority of soot particles measured in these studies were associated with nitrate, OC, and sulfate. The freshest soot particles in Mexico City were internally mixed with some inorganic species including nitrate (24%) and sulfate (75%). The fact that most of the soot was mixed with

sulfate in Mexico City suggests sulfate is produced by the oxidation of sulfur in the fuel followed by rapid condensation onto existing particles in the plume formed during the combustion process. Similar soot-sulfate mixtures have been shown to dominate the particles measured in our previous source characterization studies of fresh soot emissions from diesel trucks (24).

Temporal Characteristics of Fresh and Aged Soot. Using the ability to identify specific chemical signatures for fresh versus aged soot particles in real time, the in situ measurements were made showing the atmospheric timescale for conversion between fresh fractal to aged spherical soot particles. Fig. 1B shows a diurnal average (of 24 consecutive days) of the fractional contribution to the absorption coefficient for the fresh and aged soot particles identified in Fig. 1A. Fresh soot particles contribute most of the absorption in the early morning periods when traffic levels peak. Aged soot particles become the major absorbers ≈ 9 AM (3 h after sunrise) when photochemistry forms nitric acid and organic compounds that subsequently condense onto the soot particle surfaces (25). This conversion process transforms fresh fractal forms of soot into internal mixtures of soot, sulfate, organics, nitrate, ammonium, and water. This observation, coupled with the mass spectra showing condensed secondary species on aged soot (Fig. 1A), provides strong evidence that photochemical processing represents the dominant soot aging mechanism that occurs over a relatively short timescale of several hours in a photochemically active environment. The aging time of 3 h observed here is significantly shorter than that which had been assumed in previous modeling studies (22). In those studies, van Poppel et al. showed that if the generally accepted aging time (defined as transformation from hydrophobic to hydrophilic) of 1.15 days is decreased by a factor of 2, the forcing by soot can decrease by 20–30% because of shorter atmospheric lifetimes. However, these estimates of forcing do not account for the effects of core-shell mixing on absorption and scattering. Therefore, it is important to consider both the mixing state effect on soot absorption together with aging effects on the soot lifetime.

Optical Characterization. In the single particle mass spectrometer, the size and chemistry information is coupled to the light scattering intensity of each individual particle. We calibrated the light scattering signal to give a “partial scattering cross section” that represents the portion of the total scattering cross section measured by the light collection optics. Fig. 2 shows the measured curves of the partial scattering cross-section (R) as a function of particle diameter (D_p) for fresh and aged soot particles shown in Fig. 1A. The observed chemical changes shown in the mass spectra directly correspond to differences in the measured optical properties of these soot particles. Fig. 2 shows that fresh soot particles exhibit a scattering pattern that is distinct from aged soot particles. The aged soot particles exhibit a well-defined upper limit to the amount of scattered light as expected for a compact spherical morphology. The shape of the scattering curve for aged soot matches theoretical predictions for a strongly absorbing particle surrounded by a spherical nonabsorbing shell. However, because of their nonspherical shape, the optical properties of the fresh fractal soot cannot be fit by using this same model. The observed sphericity of the aged soot can only be explained by the soot particles having a coating of secondary species as supported by Fig. 1A. This particle morphology is consistent with other studies based on microscopic observations of mixed soot particles (11) and the previously observed collapse of a fractal structure to more compact structures upon coating soot with secondary species and water (e.g., ref. 17).

To derive core diameters (D_c), we compared the measurements in Fig. 2 with theoretical results (26) provided by the

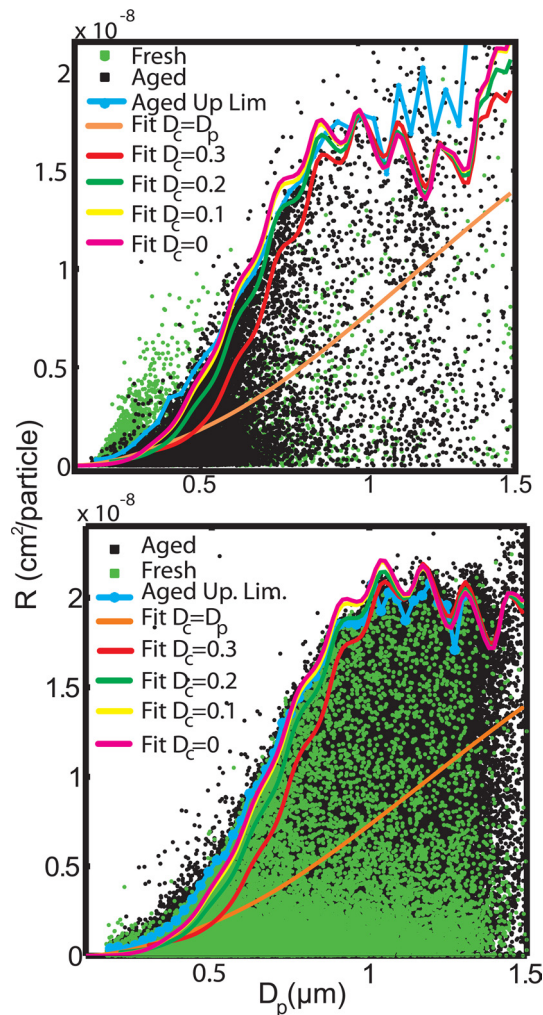


Fig. 2. Measured partial scattering cross-section (R) as a function of particle diameter (D_p). Soot particles detected in Mexico City (*Upper*) and Riverside (*Lower*) show the influence of aging on the light scattering signals. The fresh soot particles (green points) have a nonspherical shape as indicated by a large amount of scattered light at small aerodynamic diameters. The more aged particles produce a pattern similar to that obtained for spherical coated particles. For larger particle sizes in Riverside, there are more scatters at low R due to the nonsphericity of fresh soot. For comparison, core-shell model results assuming different core diameters (D_c) are plotted on top of the measured scattering data. $D_c = 0$ represents the case of particles made of pure shell material (Aged species), and $D_c = D_p$ represents the case of pure soot particles. The blue lines represent the processed data used to estimate D_c .

coated spheres model. Derived core diameter, shell refractive index, and particle effective density are shown in Table 1. In Fig. 2, the most spherical soot particles lie in the regime of a small

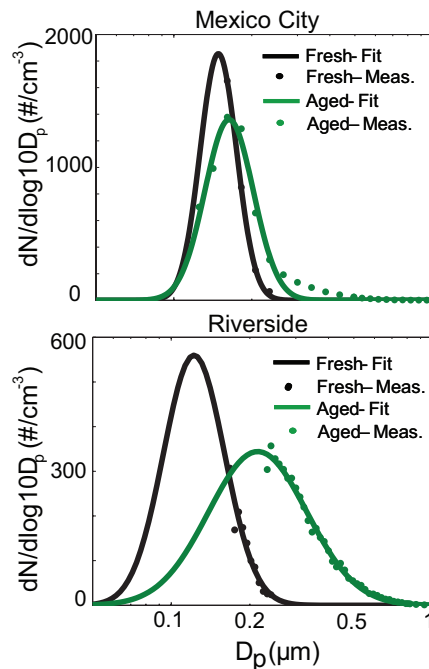


Fig. 3. Size distributions for fresh and aged soot particles. Mexico City (*Upper*) and Riverside (*Lower*) fresh soot particles occur at smaller sizes than do aged soot particles. The fresh soot distributions have been scaled down so that their total concentration is equal to the aged particle concentration. These distributions were used with the optical properties to derive integrated values for SSA and absorption enhancement.

(<0.2 μm) soot core surrounded by a large (0.2–3.0 μm) nonabsorbing coating. Bond et al. (27) have also demonstrated that this region (Region 2 in ref. 27) of large shell surrounding a small core will lead to the largest amplification of absorption (2–4 \times that of a pure soot particle). For both Riverside and Mexico City, 0.2 μm represents the upper limit for D_c to obtain agreement with our optical measurements of aged soot particles. This upper limit is reasonable given that the majority of fresh soot particles occur <200 nm.

Size Distribution. Size distributions for fresh and aged soot particles in Mexico City and Riverside are shown in Fig. 3; the count median diameters (CMD) and geometric standard deviations (GSD) for these distributions are shown in Table 1. The fresh soot types have a mode at the smallest sizes, whereas the aged soot displays a mode at larger sizes. The aged soot particles in Riverside have a much larger mode than in Mexico City, which is consistent with the observation of highly aged particles for the fall season in Riverside. For Mexico City, it was observed that the fresh soot particles had a higher count median diameter (CMD, 0.16 μm) and smaller GSD (1.2) compared with River-

Table 1. Parameters derived from measurements of fresh and aged soot particles following the procedure outlined in *Methods*

Particle set	m_s	ρ_{eff} , g/cm ³	D_c , μm	CMD, μm	GSD	AE	SSA
Riverside fresh	—	0.8 ± 0.5	—	0.12	1.3	—	—
Riverside aged	1.44 ± 0.06	1.4 ± 0.3	<0.2	0.21	1.5	1.6	0.81
Mexico City fresh	—	0.7 ± 0.5	—	0.15	1.2	—	—
Mexico City aged	1.49 ± 0.05	1.8 ± 0.3	<0.2	0.16	1.2	1.4	0.64

m_s is the shell refractive index, ρ_{eff} is the particle effective density, and D_c is the estimated core diameter for aged soot. The count median diameter (CMD) and geometric standard deviation (GSD) were derived from the measured size distributions shown in Fig 3. The absorption enhancement (AE) and single scattering albedo (SSA) were calculated using a soot refractive index, $m_c = 1.8 + 0.71i$, along with the size distributions and microphysical parameters shown in the table.

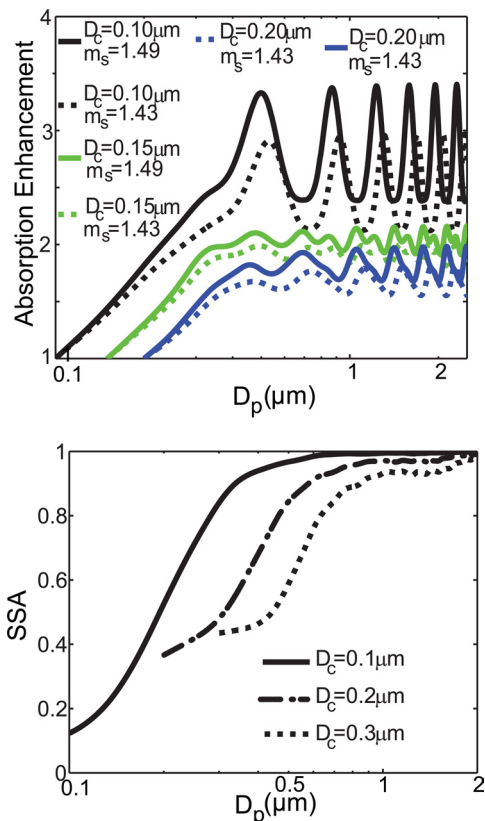


Fig. 4. Ranges for absorption enhancement and single scattering albedo (SSA) for aged soot particles derived by using a core-shell model and the measurements reported in Table 1. (Upper) The absorption enhancement depends on shell refractive index (m_s) and core diameter (D_c) as demonstrated. Riverside had a lower value of m_s (1.43) than Mexico City ($m_s = 1.49$). (Lower) SSA shows a strong dependence on D_c . The wavelength used for the calculations was 532 nm.

side (CMD, 0.12 μm ; GSD, 1.3). Comparing these size distribution parameters with those compiled by Bond et al. (27), it appears that the fresh soot modes reported here occur at the upper end of the ranges reported from a variety of likely sources. Our size distribution measurements support the result obtained from the direct fitting of the scattering data: The core size must be $<0.2 \mu\text{m}$. However, we are currently unable to constrain the lower end of the size range directly because of the incomplete measurement of the size distribution. To use these size distributions, together with derived microphysical parameters, to calculate properties such as absorption and albedo, we must make the assumption that the size distributions of the fresh particles are representative of the core distribution.

Sensitivity of Optics to Microphysics. A multitude of microphysical properties influence the optical properties of soot. When considering the climate impacts of soot, it is important to understand how absorption and scattering change with refractive index and core size measured in different geographical locations. Using the measured constraint for D_c and our best-fit microphysical parameters shown in Table 1, we calculate the size dependence of the absorption enhancement and single scattering albedo (SSA) for aged soot particles. The absorption enhancement, a direct result of coating soot with nonabsorbing species, is defined as the ratio of the absorption for the coated (aged) case to the uncoated (fresh) case. Fig. 4 shows the absorption enhancement as a function of size constrained by the optical parameters described in Table 1.

The absorption enhancement ranges from 1 (for no coating) to a maximum of 3.4 at the largest particle sizes. When the absorption is integrated to take into account both core and shell distributions, absorption enhancements of 1.6 and 1.4 are calculated for Riverside and Mexico City, respectively. The higher absorption enhancements seen for Riverside are because of the larger shell/core ratios obtained for the aged Riverside particles ($\text{CMD}_{\text{shell}}/\text{CMD}_{\text{core}} = 1.75$) compared with Mexico City ($\text{CMD}_{\text{shell}}/\text{CMD}_{\text{core}} = 1.07$). As shown in Table 1, this result is due to both a smaller core size and a larger shell size for Riverside compared with Mexico City.

Changes in chemical composition will directly affect the optical properties by modifying the refractive index. In Table 1 we show that the shell refractive indices for the particles in Mexico City and Riverside ranged from 1.44–1.49. As pointed out in Moffet et al. (23), the lower refractive index measured for Riverside is most likely due to the presence of water. Fig. 4 also shows how strongly this change in shell refractive index impacts the absorption enhancement. We find that there is up to a 30% difference between enhancements, calculated by using shell refractive indices obtained for Riverside and Mexico City, with the largest differences occurring for the largest total particle sizes and smallest core sizes. Beyond the sensitivity to shell refractive index, there is also expected to be some error because of uncertainties in the core refractive index. Bond et al. determined those errors to be $\approx 15\%$ when considering previously measured refractive indices for soot (27).

Not only does the amount of absorption change as soot takes on a coating, but the amount of scattering changes as well. As soot particles take on nonabsorbing material, the SSA increases dramatically as demonstrated in Fig. 4. For aged soot, when we integrate the SSA with respect to both core and total particle size, we obtain SSAs of 0.81 and 0.64 for Riverside and Mexico City, respectively. As was the case with absorption enhancement, the higher SSA obtained for Riverside is a result of larger coatings compared with the coatings from Mexico City. The SSA measured in Mexico City lies at the lower end of SSA reported by Marley et al. for the same sampling site and time (28). This result is reasonable given that the SSA reported here is only calculated for aged EC. The large sensitivity of soot optical properties to microphysical parameters shown in Fig. 4 and Table 1 highlights the need to accurately measure the size and refractive index for the core and shell of soot particles. Only if the microphysical properties of soot are known can their effects on radiative forcing be accurately evaluated.

Discussion

The climate impacts of soot go beyond the direct radiative effects as soot also plays a role in cloud formation. Stier et al. (29) showed that as soot particles age they become better cloud condensation nuclei and thus remain in the atmosphere for less time, which reduces their radiative impact. This lifetime effect counteracts absorption enhancement induced by thicker coatings. In some regions and/or seasons with higher levels of precipitation, this competing effect must be taken into account as it can counterbalance the additional heating imparted by adding more sulfate to the soot particles.

Because the lifetime of soot aerosols are so much shorter than CO_2 , it has been suggested that reducing soot emissions could represent a “quicker fix” for reducing atmospheric warming (14). To reduce the key uncertainties of soot impacts on climate to the level needed to guide such policy decisions, detailed measurements such as those presented here are needed to provide constraints to models. Soot shows high spatiotemporal variability, and thus more measurements at the level of those described herein are needed at more locations under a wider variety of meteorological conditions. The microphysical parameters obtained with detailed measurements can be modeled with theory and compared against in situ

ACKNOWLEDGMENTS. We thank Sharon Qin, Steve Toner, and Laura Shields for help gathering data in Riverside. Nancy Marley and Jeff Gaffney graciously provided absorption measurements. Jain Wang and Don Collins kindly provided size distribution measurements. California Air Resources

Board provided funding under Grant 04-336. R.C.M. acknowledges funding provided by the Glenn T. Seaborg postdoctoral fellowship. The Molina Center for Energy and the Environment provided support for the measurements in Mexico City.

1. Ramanathan V, et al. (2005) Atmospheric brown clouds: Impacts on South Asian climate and hydrological cycle. *Proc Natl Acad Sci USA* 102:5326–5333.
2. Twohy CH, Clarke AD, Warren SG, Radke LF, Charlson RJ (1989) Light-absorbing material extracted from cloud droplets and its effect on cloud albedo. *J Geophys Res* 94:8623–8631.
3. Riemer N, Vogel H, Vogel B (2004) Soot aging time scales in polluted regions during day and night. *Atmos Chem Phys* 4:1885–1893.
4. Ackerman TP, Toon OB (1981) Absorption of visible radiation in atmosphere containing mixtures of absorbing and non-absorbing particles. *Appl Optics* 20:3661–3668.
5. Bond TC, Bergstrom RW (2006) Light absorption by carbonaceous particles: An investigative review. *Aerosol Sci Tech* 40:27–67.
6. Chung SH, Seinfeld JH (June 1, 2005) Climate response of direct radiative forcing of anthropogenic black carbon. *J Geophys Res*, 110, D11102, 10.1029/2004JD005441.
7. Haywood JM, Roberts DL, Slingo A, Edwards JM, Shine KP (1997) General circulation model calculations of the direct radiative forcing by anthropogenic sulfate and fossil-fuel soot aerosol. *J Climate* 10:1562–1577.
8. Jacobson MZ (2001) Strong radiative heating due to the mixing state of black carbon in atmospheric aerosols. *Nature* 409:695–697.
9. Menon S, Hansen J, Nazarenko L, Luo YF (2002) Climate effects of black carbon aerosols in China and India. *Science* 297:2250–2253.
10. Stier P, Seinfeld JH, Kinne S, Boucher O (2007) Aerosol absorption and radiative forcing. *Atmos Chem Phys Diss* 7:7171–7233.
11. Jacobson MZ (2000) A physically-based treatment of elemental carbon optics: Implications for global direct forcing of aerosols. *Geophys Res Lett* 27:217–220.
12. Ramanathan V, Carmichael G (2008) Global and regional climate changes due to black carbon. *Nature Geosci* 1:221–227.
13. Sato M, et al. (2003) Global atmospheric black carbon inferred from AERONET. *Proc Natl Acad Sci USA* 100:6319–6324.
14. Bond TC, Sun HL (2005) Can reducing black carbon emissions counteract global warming? *Environ Sci Technol* 39:5921–5926.
15. Chylek P, Videen G, Ngo D, Pinnick RG, Klett D (1995) Effect of black carbon on the optical properties and climate forcing of sulfate aerosols. *J Geophys Res* 100:16325–16332.
16. Fuller KA, Malm WC, Kreidenweis SM (1999) Effects of mixing on extinction by carbonaceous particles. *J Geophys Res* 104:15941–15954.
17. Mikhailov EF, Vlasenko SS, Podgorny IA, Ramanathan V, Corrigan CE (April 15, 2006) Optical properties of soot-water drop agglomerates: An experimental study. *J Geophys Res*, 111, D07209, 10.1029/2005JD006389.
18. Schnaiter M, et al. (October 7, 2005) Absorption amplification of black carbon internally mixed with secondary organic aerosol. *J Geophys Res*, 110, D19204, 10.1029/2005JD006046.
19. Sorensen CM (2001) Light scattering by fractal aggregates: A review. *Aerosol Sci Tech* 35:648–687.
20. Schwarz JP, et al. (February 14, 2008) Coatings and their enhancement of black carbon light absorption in the tropical atmosphere. *J Geophys Res*, 113, D03203, 10.1029/2007JD009042.
21. Johnson KS, et al. (2005) Processing of soot in an urban environment: Case study from the Mexico City metropolitan area. *Atmos Chem Phys* 5:3033–3043.
22. van Poppel LH, et al. (December 24, 2005) Electron tomography of nanoparticle clusters: Implications for atmospheric lifetimes and radiative forcing of soot. *Geophys Res Lett*, 32, L24811, 10.1029/2005GL024461.
23. Moffet RC, Qin X, Rebotier T, Furutani H, Prather KA (June 27, 2008) Chemically segregated optical and microphysical properties of ambient aerosols measured in a single particle mass spectrometer. *J Geophys Res*, 113, D12213, 10.1029/2007JD009393.
24. Toner SM, Sodeman DA, Prather KA (2006) Single particle characterization of ultrafine and accumulation mode particles from heavy duty diesel vehicles using aerosol time-of-flight mass spectrometry. *Environ Sci Technol* 40:3912–3921.
25. Zheng J, et al. (2008) Measurements of HNO₃ and N₂O₅ using ion drift-chemical ionization mass spectrometry during the MCMA-2006 campaign. *Atmos Chem Phys* 8:6823–6838.
26. Bohren CF, Huffman DR (1981) *Absorption and Scattering of Light by Small Particles* (John Wiley and Sons, New York).
27. Bond TC, Habib G, Bergstrom RW (October 31, 2006) Limitations in the enhancement of visible light absorption due to mixing state. *J Geophys Res*, 111, D19204, 10.1029/2005JD006046.
28. Marley NA, Gaffney JS, Castro T, Salcido A, Frederick J (2009) Measurements of aerosol absorption and scattering in the Mexico City metropolitan area during the MILAGRO field campaign: A comparison of results from the T0 and T1 sites. *Atmos Chem Phys* 9:189–206.
29. Stier P, Seinfeld JH, Kinne S, Feichter J, Boucher O (September 19, 2006) Impact of nonabsorbing aerosols on clear-sky atmospheric absorption. *J Geophys Res*, 11, 10.1029/2006JD007147.
30. Ramanathan V, et al. (2007) Warming trends in Asia amplified by brown cloud solar absorption. *Nature* 448:575–578.
31. Gard E, Mayer JE, Morrical BD, Dienes T, Fergenson DP, Prather KA (1997) Real-time analysis of individual atmospheric aerosol particles: Design and performance of a portable ATOFMS. *Anal Chem* 69:4083–4091.
32. Song XH, Hopke PK, Fergenson DP, Prather KA (1999) Classification of single particles analyzed by ATOFMS using an artificial neural network, ART-2A. *Anal Chem* 71:860–865.
33. Moffet RC, Prather KA (2005) Extending ATOFMS measurements to include refractive index and density. *Anal Chem* 77:6535–6541.
34. Cross ES, et al. (2007) Laboratory and ambient particle density determinations using light scattering in conjunction with aerosol mass spectrometry. *Aerosol Sci Tech* 41:343–359.